Quantum Griffiths singularity in the stoichiometric heavy-fermion system $CeRh_4Al_{15}$

Rajesh Tripathi,[1,2,*] D. T. Adroja,[1,3,†] Y. Muro,[4,‡] Shivani Sharma,[1] P. K. Biswas,[1,§] T. Namiki,[5] T. Kuwai,[5] T. Hiroto,[6] A. M. Strydom,[3,7] A. Sundaresan,[2] and S. Langridge[1]

[1]*ISIS Facility, STFC, Rutherford Appleton Laboratory, Chilton, Oxon OX11 0QX, United Kingdom*
[2]*Jawaharlal Nehru Centre for Advanced Scientific Research, Jakkur, Bangalore 560064, India*
[3]*Highly Correlated Matter Research Group, Physics Department, University of Johannesburg, Auckland Park 2006, South Africa*
[4]*Center for Liberal Arts and Sciences, Faculty of Engineering, Toyama Prefectural University, Imizu 939-0398, Japan*
[5]*Graduate School of Science and Engineering, University of Toyama, Toyama 930-8555, Japan*
[6]*Research Network and Facility Services Division, National Institute for Materials Science, Tsukuba 305-0047, Japan*
[7]*Max Planck Institute CPfS, 40 Nöthnitzerstrasse, D-01187 Dresden, Germany*

(Received 30 January 2023; revised 29 September 2023; accepted 2 October 2023; published 23 October 2023)

We present a detailed investigation of the stoichiometric $CeRh_4Al_{15}$ single-crystal compound using the temperature dependence of the heat capacity $C_P(T)$, electrical resistivity $\rho(T)$, magnetic susceptibility $\chi(T)$, and magnetization $M(H)$ measurements for a magnetic field H applied in the basal plane and along the c axis. The low-temperature power-law behavior of $C/T \propto \chi \propto T^{-1+\alpha}$, the scaling behaviors of field-dependent magnetization at different temperatures up to 50 K and temperature-dependent heat capacity at various fields up to 9 T, and the T-linear resistivity are found to be consistent with the formation of quantum Griffiths singularities in the non-Fermi-liquid (NFL) regime. We further investigate the spin dynamics of a polycrystalline sample of $CeRh_4Al_{15}$, using zero-field (ZF) and longitudinal-field (LF) muon spin relaxation (μSR) measurements. ZF-μSR measurements do not reveal any sign of long-range magnetic ordering down to 70 mK. The electronic relaxation rate λ below 0.5 K increases rapidly and shows a thermal-activation-like characteristic [$T\log(\lambda) \sim T$] over the entire measured temperature range between 70 mK and 4 K, indicating the presence of low-energy spin fluctuations in $CeRh_4Al_{15}$. LF-μSR measurements show a time-field (t/H^{η}) scaling of the μSR asymmetry, indicating the quantum critical behavior of this compound. Furthermore, an inelastic neutron scattering study of the polycrystalline sample reveals two crystal field excitations near 19 and 33 meV. These features collectively provide strong evidence of NFL behavior in $CeRh_4Al_{15}$ due to the formation of the Griffiths phase close to a $T \rightarrow 0$ K quantum critical point.

DOI: 10.1103/PhysRevB.108.144427

I. INTRODUCTION

When long-range ordering of magnetic moments is suppressed by competing interactions, novel ground states of matter may emerge near the magnetic instability close to zero temperature [1]. For instance, magnetic metals near $T_N \rightarrow 0$, also called a quantum critical point (QCP), exhibit a breakdown of Fermi liquid (FL) behavior, termed non-Fermi liquid (NFL), that challenges our current understanding of strongly correlated electron systems. The existence of such NFL behavior has been proposed in many U-, Yb-, and Ce-based f-electron metals, in which the NFL behavior is found when long-range magnetic ordering is suppressed to zero temperature by a nonthermal control parameter such as tuning the chemical composition [2–4], applying pressure [5], or a magnetic field [6].

A growing number of compounds are displaying NFL behavior as a result of chemical substitution, in which magnetic ordering disappears inhomogeneously in the vicinity of the QCP [7–11]. For example, the NFL behavior was observed in $CeCu_{6-x}Au_x$ [12] and $UCu_{5-x}Pd_x$ [13], in which the NFL behavior is interpreted as a distribution of Kondo temperatures [14]. Furthermore, a number of chemically substituted systems have been described within the context of Griffiths singularities near a magnetic instability, where spin-spin interactions freeze the localized f moments, which have a low value of the Kondo temperature T_K, into clusters with a wide distribution of sizes; the larger clusters dominate the susceptibility and lead to divergent behavior of the thermodynamic quantities as the temperature is lowered [15,16]. This model has been used to explain the NFL behavior of many f-electron chemically substituted systems such as $Th_{1-x}U_xPd_2Al_3$, $Y_{1-x}U_xPd_3$, $UCu_{5-x}Pd_x$ [17], $Ce(Ru_{1-x}Rh_x)_2Si_2$ [18], and $CePtSi_{1-x}Ge_x$ [19].

On the other hand, a clean system near a QCP shows NFL behavior through the suppression of magnetic ordering following the application of hydrostatic pressure, such as in $CeIn_3$ [5] and $CePd_2Si_2$ [5,20], or even at ambient pressure (very few systems), such as in $CeNi_2Ge_2$ [21],

*rajeshtripathi@jncasr.ac.in
†devashibhai.adroja@stfc.ac.uk
‡ymuro@pu-toyama.ac.jp
§Deceased.

CeRhBi [22], UBe_{13} [23], and β-$YbAlB_4$ [24]. In these cases, a zero-temperature paramagnetic to antiferromagnetic quantum phase transition has been suggested as the possible source of the NFL behavior [25].

Recent work reporting the discovery of the stoichiometric Kondo lattice heavy-fermion system $CeRh_4Al_{15}$ suggested the possibility that this system may exhibit quantum criticality without tuning [26]. The low-temperature electronic specific heat shows a huge value of the Sommerfeld coefficient $\gamma = 2\,\mathrm{J/(mol\,K^2)}$ with no magnetic long-range order ($\theta_P = -160$ K) down to 50 mK [26]. Hence, $CeRh_4Al_{15}$ is regarded as a nonmagnetic, heavy-fermion metal close to an antiferromagnetic (AFM) instability with strong AFM fluctuations. Considering that this system is stoichiometric and devoid of chemical disorder, its low-temperature behavior differs from that of clean systems. These observations, therefore, motivated our in-depth study of single- and polycrystalline samples of $CeRh_4Al_{15}$ using a wide range of bulk and microscopic techniques at ambient pressure.

In order to understand the physics of NFL behavior in stoichiometric $CeRh_4Al_{15}$, we carefully characterize the single-crystal sample using heat capacity $C_P(T)$, electrical resistivity $\rho(T)$, magnetic susceptibility $\chi(T)$, and magnetization $M(H)$ measurements. We further investigate the spin dynamics of the $CeRh_4Al_{15}$ polycrystalline sample using muon spin relaxation (μSR) and inelastic neutron scattering (INS) measurements. Both the bulk and microscopic results indeed suggest NFL behavior driven by the quantum Griffiths phase (QGP) scenario over a wide temperature and magnetic field range. We show that the QGP in $CeRh_4Al_{15}$ emerges from the Al atoms with partial site occupancy, which locally modify the exchange interactions and lead to the formation of magnetic clusters. This results in NFL behavior, as proposed by Castro Neto *et al.* [15,17]. Furthermore, the INS shows crystal field excitations at 19 and 33 meV, indicating the localized nature of the Ce ions.

II. EXPERIMENTAL METHODS

The polycrystalline samples of $CeRh_4Al_{15}$ and $LaRh_4Al_{15}$ were prepared according to Ref. [26]. Powder x-ray diffraction (PXRD) with Mo $K\alpha$ radiation ($\lambda = 0.71073$ Å, 50 kV, 20 mA) was used to determine the phase purity and crystal structure. We prepared a high-quality single crystal of $CeRh_4Al_{15}$ using the Al-flux method. A starting composition of $Ce_1Rh_4Al_{30}$ was used, and the elements were placed in an alumina crucible and then sealed in a quartz tube with 1/3 atm of pure Ar gas. The quartz ampoule was cooled slowly from 1150 °C to 900 °C at a rate of 1 °C/h, then cooled quickly to 750 °C before centrifugation in order to avoid formation of secondary phases. For the crystal structure of $CeRh_4Al_{15}$, a single-crystal x-ray analysis was also performed by using a small piece ($89\times72\times69$ μm^3) prepared by crushing a single crystal. Diffraction data were collected at room temperature on a RIGAKU AFC11 Saturn 724+ CCD diffractometer and a Mo $K\alpha$ radiation monochromated by a VariMax confocal x-ray optics device. Structure solution and refinement were carried out using the SHELXL program (version 2018/3) [27]. The obtained atomic coordinates were standardized using the STRUCTURE TIDY program [28].

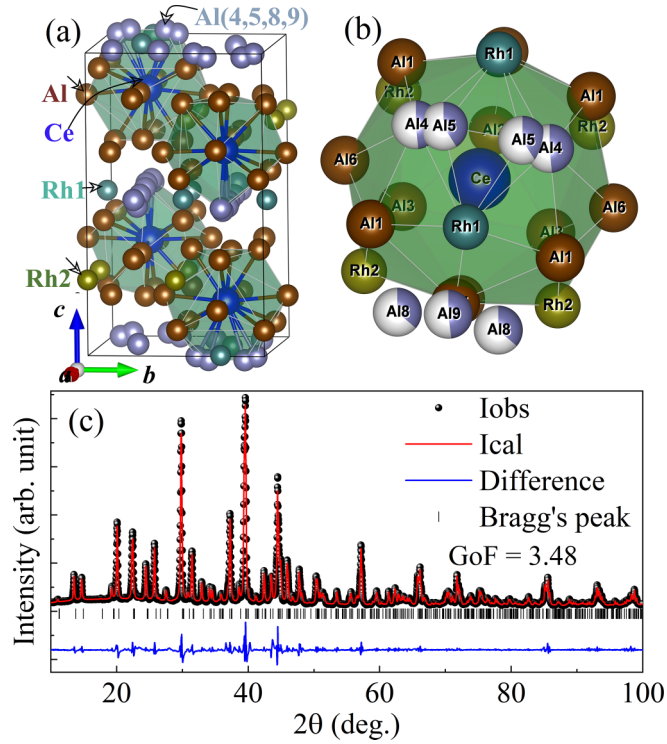

FIG. 1. (a) The crystal structure of $CeRh_4Al_{15}$. The blue, dark yellow, and wine-colored atoms are Ce, Rh, and Al, respectively. (b) The cage-type local environments of Ce, showing two Rh sites and nine Al sites. The Al sites (Al4, Al5, Al8, Al9) are partially occupied. (c) Room temperature Rietveld fitted XRD pattern of $CeRh_4Al_{15}$.

DC magnetization of a single-crystalline sample was measured down to 2 K and in high fields up to 7 T using a Quantum Design magnetic property measurement system superconducting quantum interference device with the applied magnetic field along the crystallographic c and a axes. The specific heat measurements were carried out using a physical property measurement system (PPMS) with an adiabatic demagnetization refrigerator (ADR) option down to 70 mK (adiabatic heat-pulse method) in zero field and using a ^{3}He system down to 0.4 K in various applied magnetic fields (relaxation method). Electrical resistivity measurements in the temperature ranges 2 to 300 K (AC four-terminal method) and 80 mK to 2 K (DC four-terminal method) were performed using a GM refrigerator and Quantum Design PPMS with ADR option, respectively, with the current along the crystallographic c and a axes and magnetic field in the ab plane.

Zero-field (ZF) and longitudinal-field (LF) μSR measurements on the polycrystalline sample of $CeRh_4Al_{15}$ were performed at the ISIS Neutron and Muon Source, United Kingdom, using the EMU spectrometer. For ISIS muon measurements, a crushed polycrystalline sample was mounted on a 99.999% pure silver plate using diluted GE varnish to ensure good thermal contact and then covered with a thin silver foil. We used a dilution fridge to cool the samples down to 70 mK. The μSR data were analyzed with the MANTID [29] and WIMDA [30] software.

The INS experiments on polycrystalline samples of $CeRh_4Al_{15}$ and $LaRh_4Al_{15}$ (phonon reference) were per-

TABLE I. Crystallographic parameters of $CeRh_4Al_{15}$ with $NdRh_4Al_{15}$-type tetragonal structure (space group $P4_2/nmc$) obtained from a single-crystal x-ray analysis and a Rietveld refinement of powder x-ray diffraction.

			Atomic coordinates				
Atom	x	y	z	Occupancy	U	Site	Symmetry
Ce	1/4	1/4	0.33506(2)	1	0.00571(6)	4*d*	2*mm*
Rh1	1/4	0.01207(4)	0.49810(2)	1	0.01091(6)	8*g*	.*m*.
Rh2	0.50167(2)	0.49833(2)	1/4	1	0.00544(6)	8*f*	..2
Al1	0.00326(10)	0.02576(12)	0.41532(5)	1	0.01098(13)	16*h*	1
Al2	1/4	0.01350(13)	0.18307(8)	1	0.00870(16)	8*g*	.*m*.
Al3	1/4	0.05928(16)	0.66241(7)	1	0.01093(18)	8*g*	.*m*.
Al4	1/4	0.0805(5)	0.01655(18)	0.580(5)	0.0204(5)	8*g*	.*m*.
Al5	1/4	0.1478(6)	0.0289(3)	0.420(5)	0.0204(5)	8*g*	.*m*.
Al6	1/4	0.59918(12)	0.81372(7)	1	0.00817(15)	8*g*	.*m*.
Al7	1/4	0.59993(13)	0.34405(8)	1	0.01069(17)	8*g*	.*m*.
Al8	1/4	0.6185(4)	0.0054(3)	0.338(8)	0.0158(10)	8*g*	.*m*.
Al9	3/4	1/4	0.0232(2)	0.712(13)	0.0222(9)	4*c*	2*mm*
			Lattice parameters				
	Single-crystal study					Rietveld refinement	
a (Å)	c (Å)	V (Å^3)			a (Å)	c (Å)	V (Å^3)
9.1282(4)	15.6305(6)	1302.40(12)			9.134(2)	15.605(3)	1301.9(5)
			Refinement quality				
	Single-crystal study					Rietveld refinement	
$R[F^2 > 2\sigma(F^2)]$	$wR(F^2)$	S			χ^2	R_P (%)	R_{WP} (%)
0.0436	0.1107	1.234			1.67	0.5	0.4

formed on the MERLIN time of flight spectrometer at the ISIS Neutron and Muon Source, United Kingdom [31]. The powdered samples of these materials were placed in a thin Al-foil envelope and mounted in an annular form inside thin-walled cylindrical Al cans with a diameter of 30 mm and height of 40 mm. Low temperatures down to 5 K were obtained by cooling the sample mounts in a top-loading closed-cycle refrigerator with He-exchange gas. The INS data were collected with repetition-rate multiplication using a neutron incident energy of $E_i = 75$ meV and a Fermi chopper frequency of 250 Hz, which also provided data for $E_i = 24.7$ and 12 meV. The elastic resolution (FWHM) was 5.1 meV for $E_i = 75$ meV, 0.97 meV for $E_i = 24.6$ meV, and 0.37 meV for $E_i = 12$ meV. The data are presented in absolute units [mb/(meV sr f.u.)] using the absolute normalization obtained from the standard vanadium sample measured in identical conditions.

III. EXPERIMENTAL RESULTS AND DISCUSSION

The crystal structure of $CeRh_4Al_{15}$ is presented in Figs. 1(a) and 1(b), and the PXRD pattern is presented in Fig. 1(c). The Rietveld refinement of the XRD pattern of $CeRh_4Al_{15}$ presented in Fig. 1(c) reveals the single-phase nature of the polycrystalline sample. Powder and single-crystal x-ray diffraction studies confirm that the $CeRh_4Al_{15}$ and $LaRh_4Al_{15}$ compounds crystallize in the $NdRh_4Al_{15}$-type tetragonal structure with space group $P4_2/nmc$. The obtained lattice parameters, atomic position parameters, and thermal parameters shown in Table I are in good agreement with the values reported in the literature [26]. As shown in Figs. 1(a) and 1(b), the Ce atoms are surrounded by 6 Rh and 14 Al atoms, which results in a distorted prismatic hexagonal environment of a Ce atom with 8 additional atoms capping all faces of the prism $Ce[Rh_4Al_{16}]$. These "cages" are each bounded by sharing four common vertices (Rh2) in a corrugated slab running perpendicular to the c axis.

According to an earlier structural investigation [26], $CeRh_4Al_{15}$ contains 12 crystallographic sites, including 1 cerium site, 2 rhodium sites, and 9 aluminum sites, four of which are partially occupied; Al4 splits into Al4 and Al5, and Al9 splits into two Al8 and Al9. Moreover, these unoccupied Al sites are arrayed parallel to the tetragonal a axis in Rh2-Al layer. As per Ref. [26], these four sites are not shared with any other atoms, which means that they are not due to disorder and are occupied partially.

We tried to refine the data by manually adding the disorder at a few sites. However, the refinement either diverges or does not change significantly with disordered structure. Based on the Rietveld refinement, it is hard to exclude the possibility of disorder or site mixing between Al and Rh sites. We also checked the chemical composition of single-crystal $CeRh_4Al_{15}$ with an electron probe microanalysis (EPMA; not shown here), with very good agreement between those obtained by XRD ($CeRh_4Al_{15.39}$) and EPMA ($CeRh_{3.98}Al_{15.43}$). Apparently, the disorder induced by Al atoms with partial occupancy is an intrinsic feature of the $NdRh_4Al_{15.40}$-type structure. In addition, all interatomic distances are in two different groups. The first one includes Ce-Ce, Ce-Rh, and Rh-Rh, which are close to or slightly smaller than the sum of the respective metallic single-bond radii and thereby could be regarded as chemical bonding. The second group includes Ce-Ce (>Å), Ce-Rh (>3.337 Å), and Rh-Rh (> 4.316 Å) distances significantly exceeding the sum of metallic radii of 3.66, 3.18, and 2.69 Å, respectively, clearly indicating a different environment of the magnetic Ce site.

The magnetic susceptibility measured under the applied magnetic field along the c and a axes is shown in Fig. 2(a). It is apparent from the inset in Fig. 2(a) that the data above

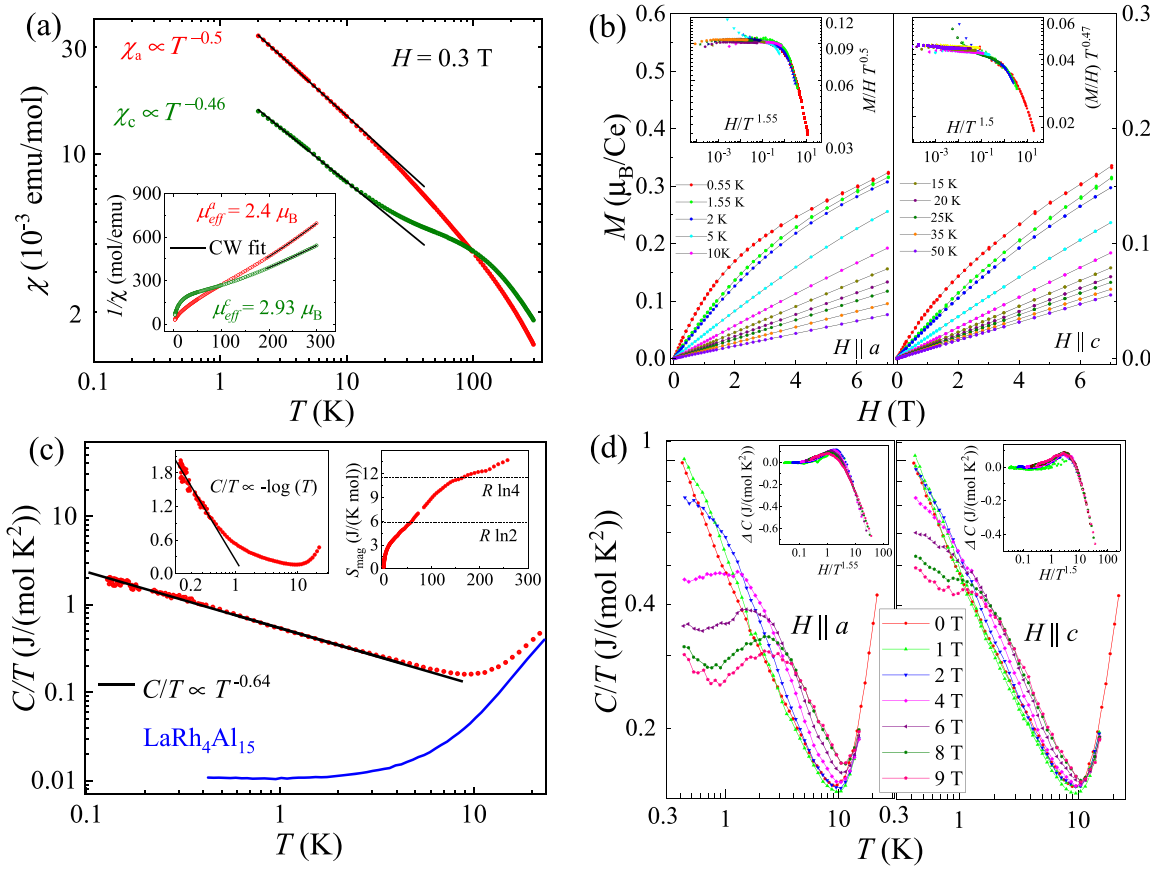

FIG. 2. (a) Log-log plot of the magnetic susceptibility vs temperature of $CeRh_4Al_{15}$ under applied magnetic field along the c and a axes. The solid lines are fitted to the data with $\chi \propto T^{-1+\alpha_\chi}$ behavior. The inset shows inverse susceptibility, with the solid lines representing Curie-Weiss behavior at high temperatures. (b) Magnetization as a function of field along a and c axes at various temperatures. The insets show $(M/H)T^\alpha$ vs $g(H/T^\beta)$ scaling in the temperature range $0.55 \leqslant T \leqslant 50$ K. (c) Low-temperature specific heat of $CeRh_4Al_{15}$ and $LaRh_4Al_{15}$ on a log-log plot. The solid line is a fit to the data with $C/T \propto T^{-1+\alpha_C}$ behavior. The left inset shows C/T vs $\log T$ and is fitted by $C/T \sim -\log T$ (solid line). The right inset shows the magnetic $(4f)$ entropy S_{mag} as a function of temperature obtained from the heat capacity data as described in the text. (d) Low-temperature specific heat of $CeRh_4Al_{15}$ (on a log-log scale) at varying fields applied parallel to the a and c axes. The insets show $\Delta C = C(H)/T - C(0)/T$ vs $f(H/T^\beta)$ scaling in the temperature range $0.4 \leqslant T \leqslant 10$ K.

100 K along both directions are best described by a modified Curie-Weiss law with the parameters $\chi_0^a = 5\times10^{-4}$ emu/mol, $\mu^a_{\rm eff} = 2.4\ \mu_B$, and $\theta^a_P = -74$ K for $H \parallel a$ and $\chi_0^c = 6\times10^{-4}$ emu/mol, $\mu^c_{\rm eff} = 2.9\,\mu_B$, and $\theta^c_P = -139$ K for $H \parallel c$. The effective magnetic moments are comparable to or slightly larger than the free Ce^{3+} ion value of $2.54\,\mu_B$ for applied magnetic field along the a and c-axes, respectively. The sign of the Weiss temperature suggests AFM correlations of the Ce moments. The susceptibility is very anisotropic along the two different crystallographic directions. At the lowest temperature, it reaches a value for an applied magnetic field along the basal plane that is two times higher than the susceptibility with an applied field along the c axis. This observation suggests that the anisotropic AFM spin fluctuations are much stronger along the basal planes. The interesting observation is the crossover seen in the temperature dependence of the susceptibility of the a and c axes near 100 K, indicating the change from an easy c axis to an easy plane anisotropy.

Upon cooling, $\chi(T)$ exhibits a power-law behavior over nearly a decade in temperature $2 \leqslant T \leqslant 10$ K, as $\chi(T) = a \times T^{-1+\alpha_\chi}$, with $\alpha_\chi = 0.5$ and 0.54 for H applied in the basal plane and along the c axis, respectively, with no evidence of magnetic order down to 2 K. This type of power-law behavior of $\chi(T)$ is observed for several NFL systems such as CeRhBi [22,32,33] and suggests $CeRh_4Al_{15}$ is located near a QCP.

The scaling of field-dependent magnetization data at different temperatures and temperature-dependent heat capacity data at various fields can provide further insight into the origin of the observed NFL behavior [34,35].

The magnetization data presented in Fig. 2(b) unveil a scaling behavior $M/H = T^{-\alpha} g(H/T^\beta)$. The data collapse on one universal function with α (β) = 0.5 (1.55) and 0.47 (1.47) for the applied magnetic field along the a and c axes, as shown in the insets in Fig. 2(b). The observed value of α is consistent with the power-law exponent $\alpha_\chi = 0.5$ and 0.46 for the respective field directions. The same scaling holds for the specific heat, as discussed below.

We further performed zero-field heat capacity measurements on the single-crystal sample of $CeRh_4Al_{15}$, as shown in Fig. 2(c). The low-temperature heat capacity diverges with decreasing temperature with a power-law-like behavior, $C(T)/T = aT^{-1+\alpha_C}$, with $\alpha_C = 0.44$ in the temperature

range $0.1 \leqslant T \leqslant 7$ K. Similar power-law behavior in the heat capacity has been reported for some chemically substituted systems exhibiting NFL behavior with strong disorder near a critical concentration, also called Griffiths singularities, e.g., $Ce_{1-x}Th_xRhSb$ [36] and $Ce(Cu_{1-x}Co_x)_2Ge_2$ [4]. Similar power-law behavior in the low-temperature heat capacity has also been seen for some stoichiometric NFL systems like $CeInPt_4$ [37]. Here, it should be noted that our data diverge more strongly than the standard $C/T \sim -\log T$ behavior found in many heavy-fermion systems displaying NFL behavior near an AFM QCP [7,38]. It can be seen in the left inset in Fig. 2(c) that C/T is roughly proportional to $-\log T$ over a narrow temperature range from 0.13 to 0.7 K. Our data are also in marked contrast to the $C_{4f}/T \propto 1 - a\sqrt{T}$ predicted by the spin-fluctuation theory at the AFM QCP in three dimensions [1,7]. Furthermore, the calculated heat capacity of the NFL system UCu_4Ni using the Kondo disorder model exhibits $C/T \propto -\log T$ [39], which is not the case for $CeRh_4Al_{15}$, and hence, we rule out the possibility of a Kondo disorder model for $CeRh_4Al_{15}$.

The electronic coefficient of the specific heat $\gamma = 23(6)$ mJ/(mol K^2) is obtained from a linear fitting of the C/T versus T^2 data in the range of $10 \leqslant T \leqslant 15$ K (fit not shown), reflecting the moderate heavy-fermion behavior in $CeRh_4Al_{15}$. With $\gamma = 10.0(5)$ mJ/(mol K^2) for $LaRh_4Al_{15}$, we estimate the renormalized quasiparticle mass in $CeRh_4Al_{15}$ [$\gamma(CeRh_4Al_{15})/\gamma(LaRh_4Al_{15}) \sim 2.3$] to be $m^* \sim 2.3m_e$, where m_e is the free electron mass.

The magnetic entropy S_{mag}, calculated by integrating C_{4f}/T versus T, where $C_{4f} = C(CeRh_4Al_{15}) - C(LaRh_4Al_{15})$, is shown in the right inset in Fig. 2(c). The value of entropy is $0.3R\ln 2$ at $T = 4$ K and $R\ln 2$ at 56 K. The reduced value of the magnetic entropy suggests the presence of Kondo screening of the f moment by the conduction electrons. The full entropy expected for the $J = 5/2$ multiplet of Ce^{3+} is recovered at room temperature, which indicates that, overall, the crystal electric field (CEF) splitting energy is close to 300 K.

Figure 2(d) shows the variation of $\log C/T$ vs $\log T$ with fields $H \leqslant 9$ T applied parallel to the c and a axes. The low-temperature upturn for $H = 0$ transforms into a maximum with increasing H. The data for $H > 0$ show a broad maximum, which shifts to higher temperatures with increasing H, which is typical behavior of Kondo systems under magnetic field. The evolution of the Schottky specific heat results from the splitting of the CEF ground state doublet by the Zeeman effect via the excited Ce^{3+} ($4f^1$, $J = 5/2$) state that splits into three Kramers doublets. The change in the low-temperature heat capacity is larger for the magnetic field parallel to the basal plane than for the field along the c axis, leading to a gradual recovery of the properties of a FL, in agreement with $\rho_a(T)$ discussed in the next section. A very similar behavior was reported in other NFL compounds [21].

The specific heat data measured under various fields applied parallel to the c and a axes exhibit the same scaling that we observed for the magnetization data. The insets in Fig. 2(d) show that in the temperature range $0.4 \leqslant T \leqslant 10$ K, our data are consistent with the scaling relation $\Delta C = C(H)/T - C(0)/T = f(H/T^\beta)$, with $\beta = 1.55$ and 1.5 determined from the magnetization scaling for the field applied parallel to the a and c axes, respectively. Because an exponent β greater than 1 indicates a non-single-impurity effect [34], our scaling analysis rules out a single-ion effect as a possible reason for the NFL behavior and may be taken as further evidence of the Griffiths phase as a possible origin for the NFL behavior.

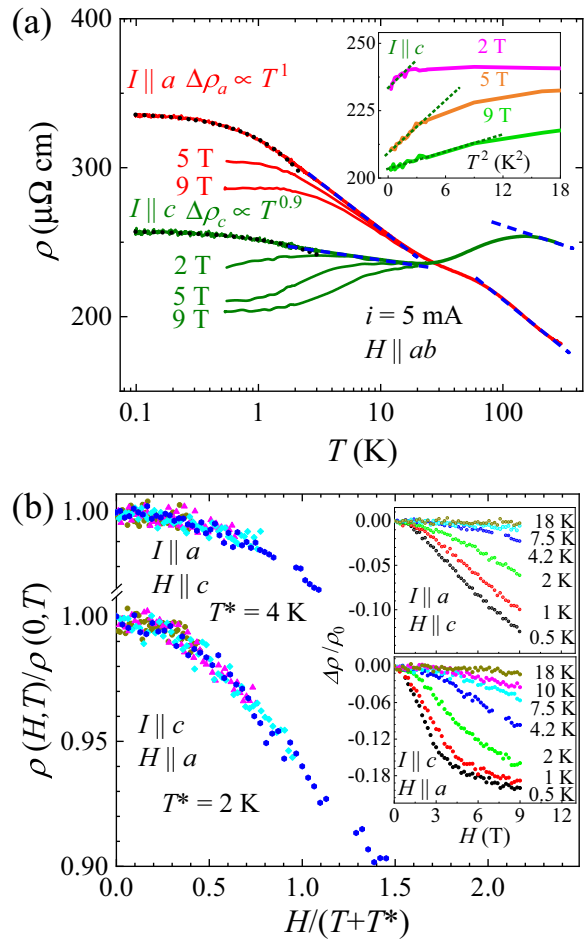

FIG. 3. (a) Temperature dependence of the electrical resistivity and its magnetic field response down to 0.1 K with the current flowing along the a and c axes and the magnetic field applied within the crystallographic ab plane on a log scale. It should be noted that there is a factor of 10 missing in the absolute value of the resistivity of the polycrystalline sample of $CeRh_4Al_{15}$ reported in Ref. [26]. The dotted black lines represent the power-law fit as discussed in the text. The blue dashed lines represent the $-\log(T)$ behavior. The inset shows a resistivity vs T^2 plot for various applied magnetic fields for current flowing along the c axis, indicating the validity temperature range of the T^2 law. (b) Normalized resistivity as a function of $H/(T + T^*)$, where T^* is the characteristic temperature, showing the scaling behavior in the temperature range 4 to 18 K. Insets: The normalized resistivity plotted as a function of applied magnetic field for $I \parallel a$ and $H \parallel c$ (top inset) and $I \parallel c$ and $H \parallel a$ (bottom inset).

Figure 3(a) shows the temperature evolution of the electrical resistivity and its magnetic field response from 0.1 to 300 K with the current flowing along the a (ρ_a) and c (ρ_c) axes and the magnetic field applied within the crystallographic ab plane. The resulting ρ_a and ρ_c are highly anisotropic, with similar behavior along both directions. For both directions at high temperatures, ρ exhibits $-\log(T)$ behavior [blue dashed

lines in Fig. 3(a)], followed by a broad maximum. Below these maxima, both ρ_a and ρ_c keep increasing logarithmically with decreasing temperature, followed by a saturationlike behavior at low temperatures.

The low-temperature Kondo coherence seems to be absent, and the resistivity keeps increasing with decreasing temperature for $CeRh_4Al_{15}$. Very similar behavior of the low-temperature resistivity has been observed in the NFL material $U_{0.2}Y_{0.8}Pd_3$ [34]. The Griffiths phase driven by the structural disorder and the value of the local microscopic exchange constants yield an effective Kondo temperature T_K^{eff} (this is an upper limit of the ground state T_K). There is a possibility of $T_K \to 0$ K, as suggested by the breakdown of the magnetoresistance (MR) scaling in Fig. 3(b) below 4.2 K (discussed below). The Kondo coherence in resistivity should appear below T_K; however, there are some clusters in $CeRh_4Al_{15}$ with unscreened local moments due to randomness called rare regions in the Griffiths scenario, yielding the negative linear term in the resistivity and giving rise to NFL behavior [40,41].

It is important to note that at room temperature ρ_a is significantly smaller than ρ_c and the anisotropy switches at a lower temperature, which is consistent with the magnetic susceptibility and can be explained by the coupling of the conduction electrons with the components of the magnetic moment (i.e., a larger component of the moment will lead to stronger scattering).

In zero field, a T^2 dependence of the low-temperature resistivity, characteristic of FL behavior, is absent in the two principal directions; instead, $\rho(T)$ varies linearly with temperature [$\Delta\rho(T) \sim T^{\epsilon}$, with $\epsilon_a = 1$ and $\epsilon_c = 0.9$; Fig. 3(a)] and is characteristic of an NFL state [42–45]. Moreover, the effect of the magnetic field has a very interesting effect on the low-temperature resistivity. With increasing magnetic field, the low-temperature diverging resistivity is lost only for ρ_c [$H \parallel ab$ with the current along c direction; Fig. 3(a)], and the temperature dependence follows a T^2 law, like a typical FL [inset in Fig. 3(a)]. The range of temperatures in which FL behavior is observed increases with increasing field, which is similar to what is observed in the stoichiometric compound $CeNi_2Ge_2$ [46]. However, ρ_a saturates like in the zero-field case even in a field of 9 T, although with a decreased saturation value.

The insets in Fig. 3(b) show the MR $\rho(H)$ vs magnetic field at different T for current parallel to the a ($H \parallel c$) and c ($H \parallel a$) directions. The MRs for both directions are negative over the entire temperature range of $0.55 \leqslant T \leqslant 18$ K. In the paramagnetic region, the negative MR is due to the freezing out of spin-flip scattering in a Kondo compound by the magnetic field. However, the positive MR in the ordered state is consistent with the AFM nature of the magnetic ordering [47]. Therefore, the behavior of the negative MR could be attributed to the absence of magnetic ordering in the Kondo lattice system $CeRh_4Al_{15}$. In order to estimate T_K, the normalized MR $\rho(H)/\rho(0)$ plotted as a function of $H/(T + T^*)$ is presented in Fig. 3(b). This allows us to scale the MR data measured at different temperatures (from 4.2 to 18 K) onto a single curve. Here, T^* is the characteristic temperature, which is an approximate measure of T_K [48]. Thus, estimated values of $T_K = 4$ and 2 K for $I \parallel a$ and $H \parallel c$ and $I \parallel c$ and $H \parallel a$, respectively, are in excellent agreement with $T_K = 3.1(3)$ K reported for the polycrystalline sample [26]. However, the dataset corresponding to lower temperatures, below 4 K, deviates from this model. We anticipate that this deviation might arise from a varied distribution of the Kondo temperature, a factor accountable for the observed quantum Griffiths singularity in $CeRh_4Al_{15}$.

All these results confirm the NFL ground state of the $CeRh_4Al_{15}$ single crystal and lead to further examination using a microscopic technique such as muon spin relaxation measurements.

To further probe the nature of the ground state observed from the thermal and transport measurements at low T, we carried out ZF- and LF-μSR measurements down to 70 mK. μSR is a powerful local probe that is able to detect tiny magnetic moments with an average ordered moment size of $0.005\,\mu_B$ (or higher) and can distinguish the random static fields associated with, for example, the dipolar coupling of the muon and quasistatic nuclear moments and dynamically fluctuating fields associated with electronic spin fluctuations. Details of the μSR technique can be found in Ref. [49]. The time-dependent ZF-μSR spectra of $CeRh_4Al_{15}$ collected at various temperatures between 0.07 and 4 K are displayed in Fig. 4(a). At high temperatures, the μSR spectra show faster depolarization, a minimum near 5 μs, and recovery at a higher time, which is a typical behavior arising from the nuclear moment contribution. When cooling below 1 K a weak temperature dependence of the relaxation rate is observed, which is due to electronic relaxation. However, neither the oscillatory signal nor a 2/3 loss of the initial asymmetry of the muon polarization is observed. This behavior suggests the absence of a well-defined or disordered static magnetic field (from electronic moments) at the muon stopping site and hence rules out any possibilities of long-range magnetic ordering or spin freezing due to Ce^{3+} moments.

The ZF-μSR spectra were successfully fitted to the following muon spin relaxation function:

$$A_z(t) = A_0 G_{\text{KT}}(t) \times \exp(-\lambda t) + A_{\text{BG}}, \tag{1}$$

where A_0 is the initial asymmetry, λ is the muon spin relaxation rate accounting for the dynamic magnetic fields due to fluctuating electronic moments, A_{BG} is a constant background arising from muons stopping on the silver sample holder, and G_{KT} is the static Kubo-Toyabe function describing the muon spin depolarization with a rate of σ_{KT} caused by randomly oriented ^{103}Rh and ^{27}Al nuclei and is given by [50]

$$G_{\text{KT}}(t) = \frac{1}{3} + \frac{2}{3}[1 - (\sigma_{\text{KT}}t)^2] \exp\left(\frac{-\sigma_{\text{KT}}^2 t^2}{2}\right). \tag{2}$$

The fits to the spectra by Eq. (1) are shown by the solid curves in Fig. 4(a). The fitting parameter λ determined from the best fits is displayed in Fig. 4(b). The value of σ_{KT} was found to be $\sim$0.295 μs^{-1} from fitting the spectra at 4 K, and this value was found to be nearly temperature independent down to 70 mK. A_{BG} (= 0.02) was estimated from 70 mK data and was kept fixed to fit all the other spectra.

It can be seen from Fig. 4(b) that λ exhibits a sharp increase as T decreases, without any sign of static magnetic ordering down to 70 mK. λ shows an activated behavior, $\lambda(T) = \lambda_0 \exp(-E_g/k_B T)$, or, equivalently, $T \log(\lambda) = T \log(\lambda_0) - E_g/k_B$, where E_g is the energy gap and k_B is Boltzmann's constant. A linear fit of the $T \log(\lambda)$ versus T plot [inset

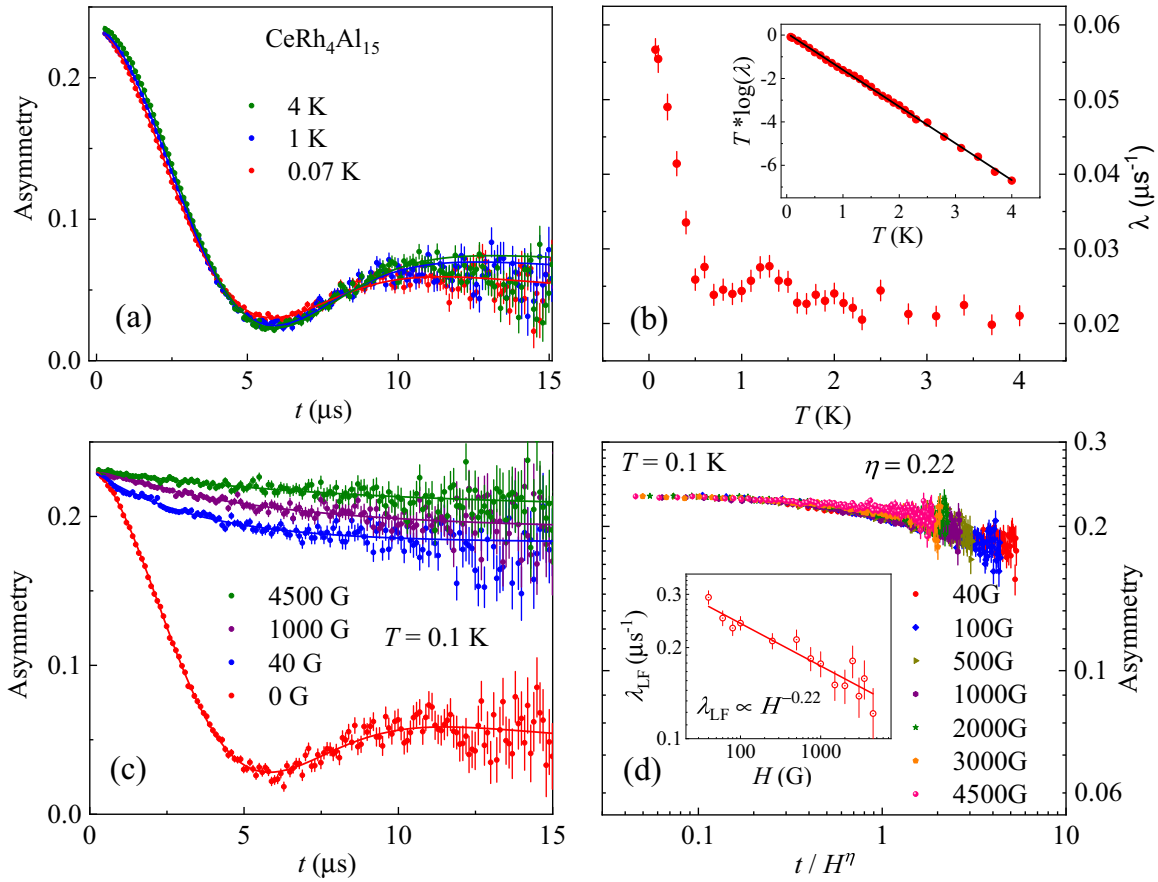

FIG. 4. (a) ZF-μSR spectra of $CeRh_4Al_{15}$ at representative temperatures. The solid lines are the fitted curves (see the text for details). (b) Temperature dependence of the muon spin relaxation rate λ. The inset describes an activationlike behavior of λ, i.e., $\lambda(T) = \lambda_0 \exp(-E_g/k_B T)$, over a given temperature range. (c) LF-μSR spectra at 0.1 K at different fields up to 4500 G. The solid lines are the fitted curves (see the text for details). (d) Time-field scaling of the asymmetry function $A(t)$ vs t/H^η at 0.1 K. The inset shows the log-log plot of λ_{LF} vs H with a solid line representing the power-law behavior.

in Fig. 4(b)] yields $E_g = 90(1)$ mK. Thus, the spin dynamics seem to be thermally activated, indicating the presence of low-energy spin fluctuations in $CeRh_4Al_{15}$. Very similar behavior was also observed for the stoichiometric NFL systems $CeInPt_4$ and CeRhBi, with activation energies of 2.9 and 140(3) mK, respectively [22,37].

We further carried out LF-dependent measurements in order to determine the dynamics of the electronic magnetic moment fluctuations in $CeRh_4Al_{15}$. When a small LF (about 25 G) is applied, the observed weak contribution from the nuclear magnetic moments observed in the ZF signal is eliminated. On the other hand, a large LF is needed to decouple the muon depolarization from the internal field arising from the fluctuating electronic spins. The representative LF spectra are displayed in Fig. 4(c). It is seen that even at 4500 G LF it is not sufficient to suppress the muon relaxation at 0.1 K completely. This reveals that the magnetic ground state is entirely dynamic at the base temperature. However, field-dependent spectra at $T = 4$ K (not shown here) behave as expected for the high-temperature paramagnetic state. The LF spectra measured at 0.1 K under several magnetic fields ($\geqslant 40$ G) can also be modeled by Eq. (1) with $G_{KT}(t) = 1$. The obtained λ_{LF} as a function of the field is shown in the inset in Fig. 4(d). The variation of $\lambda_{LF}(H)$ can be represented by a power-law behavior with a power exponent of $-0.22(3)$.

Furthermore, our LF-μSR data follow characteristic time-field scaling $A(t, H) = A(t/H^\eta)$, where the exponent η provides information about spin-spin dynamical autocorrelation [13,50–52]. By observing the time-field scaling, independent information about the nature of the spin autocorrelation function $q(t) = \langle S_i(t) S_i(0) \rangle$ can be obtained. In an inhomogeneous system, $q(t)$ is theoretically predicted to exhibit a power-law behavior for $\eta < 1$ and stretched exponential behavior for $\eta > 1$ [52,53]. The asymmetry as a function of the scaling variable t/H^η at 0.1 K is shown in Fig. 4(d). The best scaling of the overall data can be obtained with $\eta = 0.22$ for H_{LF} data up to 4500 G. The scaling exponent η is less than 1, implying that the spin autocorrelation function $q(t)$ is well approximated by a power law rather than stretched-exponential or exponential behavior ($\eta > 1$) [52]. A value of $\eta = 1/2$ is also predicted by the mean-field model of a disordered Kondo alloy at a QCP [54,55].

Similar time-field scaling has also been observed in chemically substituted systems near a QCP such as $UCu_{5-x}Pd_x$, $CePtSi_{1-x}Ge_x$, and $CePd_{0.15}Rh_{0.85}$ and in stoichiometric NFL systems like CeRhBi [22,52,56], as well as in the spin glass

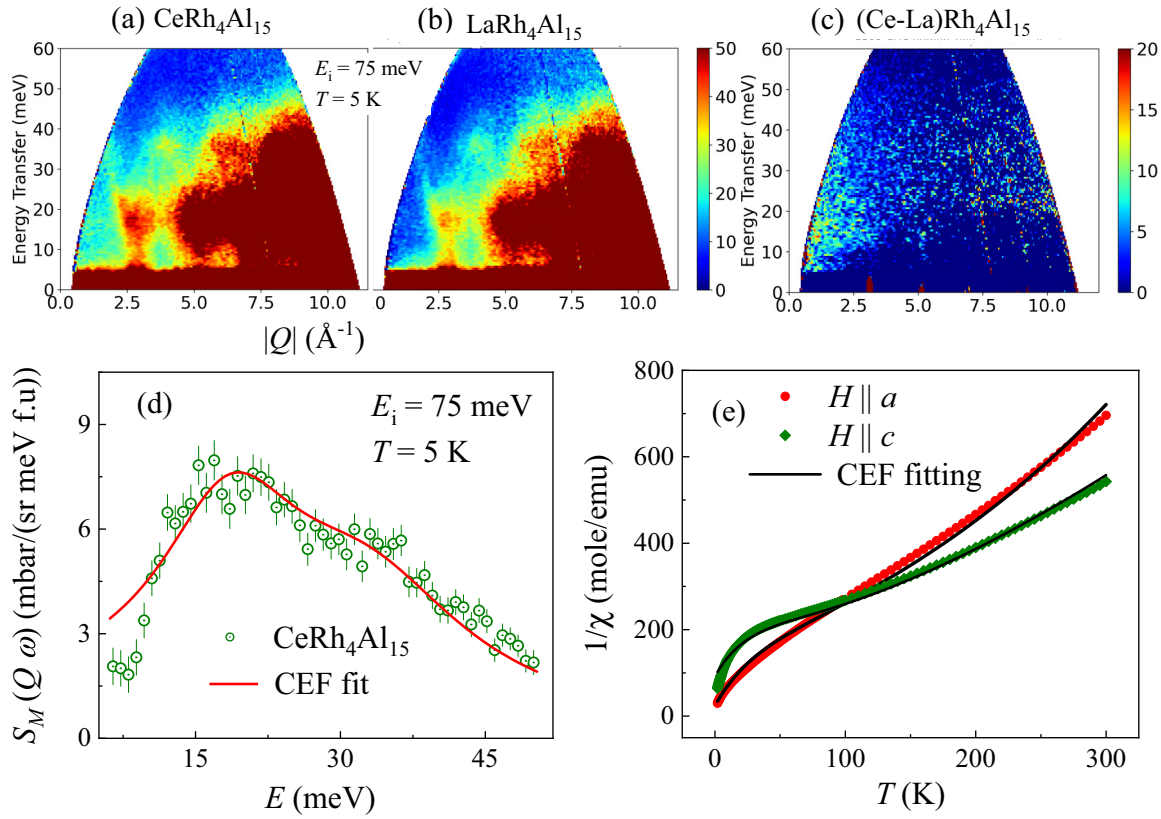

FIG. 5. Powder averaged neutron scattering intensity plots measured with incident energy $E_i = 75$ meV at temperature $T = 5$ K for (a) $CeRh_4Al_{15}$ and (b) $LaRh_4Al_{15}$. (c) The estimated magnetic scattering intensity from subtracting the phonon contribution, $CeRh_4Al_{15} - LaRh_4Al_{15}$. (d) Magnetic INS response of $CeRh_4Al_{15}$ at 5 K after subtracting the phonon contribution from $LaRh_4Al_{15}$. The solid line shows the fit based on the CEF model (see text). (e) Single-crystal inverse susceptibility versus temperature for the applied field along a and c directions. The solid black lines show the fit based on the CEF model (see text).

system AgMn (0.5 at. %) above T_g [57]. The observed value of $\eta = 0.22$ for $CeRh_4Al_{15}$ is less than the values observed for $UCu_{3.5}Pd_{1.5}$ ($\eta = 0.7$), CeRhBi ($\eta = 0.8$), and $CePtSi_{1-x}Ge_x$ ($\eta = 1.6$ for $x = 0$ and 0.1) but comparable to the value observed for UCu_4Pd ($\eta = 0.35$).

In order to investigate the nature of $4f$-electron and single-ion CEF anisotropy, we performed high-energy INS measurements on the polycrystalline sample of $CeRh_4Al_{15}$ [Fig. 5(a)]. We also measured $LaRh_4Al_{15}$ to estimate the phonon scattering [Fig. 5(b)]. The magnetic scattering of the 75 meV data was estimated using direct subtraction of the scattering of the nonmagnetic reference $LaRh_4Al_{15}$ from the Ce data as $S(Q,\omega)_M = S(Q,\omega)_{Ce} - \alpha S(Q,\omega)_{La}$. Here, α (= 0.87) is the scaling factor obtained from the ratio of the total scattering cross section of the Ce to La compounds. In this procedure, we found that the phonon modes were still present in the magnetic scattering at high Q. Hence, we used $\alpha = 1.1$ to estimate the magnetic scattering, which resulted in a better estimation of the magnetic scattering. The estimated magnetic scattering is presented in Figs. 5(c) and 5(d). We also estimated the magnetic scattering using another method [58], i.e., $S(Q,\omega)_M = S(Q,\omega,\text{low } Q)_{Ce} - S(Q,\omega,\text{high } Q)_{Ce}/[S(Q,\omega,\text{high } Q)_{La}/S(Q,\omega,\text{low } Q)_{La}]$. We found magnetic scattering (data not shown) very similar to that in Fig. 5(d). Figure 5(d) shows two well-defined magnetic excitations centered near 19 and 33 meV, which we attribute to the CEF excitations of the ground state multiplet $J = 5/2$ of Ce^{3+} splitting into three CEF doublets. The linewidth of the observed CEF excitations is higher than the instrument resolution ($\Delta E = 3.8$ and 3.0 meV at 19 and 33 meV energy transfer, respectively). We do not have a clear explanation for this at present, but there are two possibilities: (i) The value of the high-temperature Kondo temperature T_K^{high} is 85 K, which is reflected in the broader linewidth. (ii) We have some unoccupied Al sites, which will also result in a distribution of the CEF potential and hence a broader linewidth.

Now we present the analysis of INS data based on the CEF model. The symmetry for the Ce site is approximated by tetragonal point symmetry ($m2m$, C_{4v}), which results in two CEF excitations in the paramagnetic state. The CEF Hamiltonian for the tetragonal point symmetry (C_{4v}) of the Ce^{3+} ions is given by

$$H_{CEF} = B_2^0 O_2^0 + B_4^0 O_4^0 + B_4^4 O_4^4, \tag{3}$$

where B_n^m are CEF parameters and O_n^m are the Stevens operators [59]. B_n^m parameters need to be estimated by fitting the experimental data, such as single-crystal susceptibility and/or INS data. For the analysis of INS data, we use a Lorentzian line shape for the inelastic excitations.

H_{CEF} causes the sixfold degenerate Ce^{3+} ($4f^1$, $J = 5/2$) state to split into three Kramers doublets. In order to obtain a

set of CEF parameters that consistently fit the INS data and single-crystal susceptibility, we performed a simultaneous fit of INS at 5 K and the single-crystal susceptibility data using the MANTID software [29]. Fits to the INS data at 5 K and $\chi(T)$ from 5 to 300 K are shown by the solid curves in Figs. 5(d) and 5(e). The CEF parameters obtained from the simultaneous fit are (in meV) $B_2^0 = -0.6725(5)$, $B_4^0 = 0.08515(8)$, and $B_4^4 = -0.2576(4)$. The analysis gives the first excited doublet (Δ_1) at 18.55 meV and the second excited doublet (Δ_2) at 32.67 meV [the fitted values are $\lambda = -23(1)$ and $-87(2)$ and $\chi_0 = -0.0010(3)$ and $-0.0005(1)$ emu/mol for H along a and c, respectively].

IV. DISCUSSION

Quantum Griffiths phases are generally detected in inhomogeneous systems near a QCP driven by chemical substitution and are responsible for FL breakdown. More surprisingly, here, in stoichiometric $CeRh_4Al_{15}$, the low-temperature NFL behaviors are observed to be favored by the quantum Griffiths scenario, which is described as the power-law behavior of (i) the electrical resistivity, which increases from a residual value as $\rho \sim T^{\epsilon}$, with $1 \leqslant \epsilon < 2$; (ii) the Sommerfeld coefficient $\gamma = C/T \sim T^{\alpha_C}$; (iii) the DC magnetic susceptibility $\chi \sim T^{\alpha_\chi}$; and (iv) the scaling behavior of the magnetization $M/H = T^{-\alpha} g(H/T^{\beta})$ and heat capacity $\Delta C = C(H)/T - C(0)/T = f(H/T^{\beta})$. We observe that there is a disparity between the estimated values of α_χ and α_C, inferred from the fits to magnetic susceptibility and heat capacity data, respectively. Similar discrepancies were also observed by Castro Neto and colleagues [17] and were attributed to magnetocrystalline anisotropy and the preferred crystalline orientation in single-crystalline samples.

Moreover, the scaling analysis of the temperature-dependent magnetization and magnetic-field-dependent specific heat data yields an exponent β greater than 1. The fact that the magnetic field scales with a scaling dimension greater than 1 indicates that a single-impurity interpretation is not valid in our case: single-impurity fixed points typically have scaling dimensions smaller than 1 [34,35]. This may be taken as further evidence of a Griffiths phase as a possible origin for the NFL behavior in $CeRh_4Al_{15}$. Building on this observation, we pose the question of whether $CeNi_2Ge_2$, characterized by a scaling factor greater than 1 [60], could potentially host a Griffiths phase. Furthermore, we consider the possibility that the distinct observations of non-Fermi liquid behavior in $CeNi_2Ge_2$, possibly arising from tiny off-stoichiometries of Ni and Ge, could be associated with the Griffith phases. We believe that it would be of great interest to reinvestigate $CeNi_2Ge_2$ in the context of this emerging perspective in future studies.

Now, we propose that the quantum Griffiths phase in $CeRh_4Al_{15}$ emerges from the defects in the crystal structure as the Al sites are not 100% occupied, which locally modifies the exchange interactions in this undoped compound and also disorder in the CEF potential. The latter has been observed and confirmed through broad CEF excitations. We anticipate that such defects could result in the formation of magnetic clusters in proximity to the QCP leading to NFL behavior, such as those resulting from impurities or the bond disorder induced quantum Griffiths phase proposed by Castro Neto *et al.* [15,17].

V. CONCLUSIONS

In conclusion, we reported a comprehensive study of electrical transport, magnetic susceptibility, and heat capacity measurements on a single-crystal sample of $CeRh_4Al_{15}$ together with μSR and neutron scattering experiments on the polycrystalline sample. A significant deviation of the physical properties from a FL behavior, such as $\rho \sim T^{\epsilon}(1 \leqslant \epsilon < 2)$, $C/T \sim T^{\alpha_C}$, and $\chi \sim T^{\alpha_\chi}$, with $\alpha_C \sim \alpha_\chi < 1$, was observed, which has been attributed to the NFL behavior in proximity to the QCP. The observed values of the exponents $\alpha < 1$ are consistent with the power-law Griffiths singularity proposed by Castro Neto *et al.* [15,17]. Moreover, the scaling analysis of the temperature-dependent magnetization and magnetic-field-dependent specific heat data yielded an exponent β (>1) that may be taken as further evidence of a Griffiths phase as a possible origin for the NFL behavior.

The temperature dependence of the ZF-μSR dynamic relaxation rate λ exhibits a thermal-activation-like characteristic ($T \log \lambda \sim T$) over the entire measured temperature range, indicating the presence of low-energy spin fluctuations in $CeRh_4Al_{15}$. The LF-μSR data at 100 mK exhibit a time-field scaling with an exponent $\eta = 0.22(1)$, which suggests that the spin-spin autocorrelation function has a power-law behavior. The INS study showed two broad CEF excitations. The simultaneous analysis of INS and single-crystal susceptibility based on the CEF model explained the observed crossover behavior of the temperature dependence of single-crystal susceptibility between the a and c axes.

The XRD analysis further confirmed that the structural disorder is due to partial occupancy of some of the Al sites, which could affect the physical properties and hence results in the observed behavior. We thus propose that the Griffiths phase crucially controls the low-temperature spin dynamics and is responsible for the NFL behavior. Our study provides evidence of the presence of such clusters inside a paramagnetic environment even in the undoped compound.

ACKNOWLEDGMENTS

We gratefully acknowledge the ISIS facility for the beam time on MERLIN (RB1920702) [61] and EMU (RB2010778) [62]. D.T.A. would like to thank the Royal Society of London for International Exchange funding between the United Kingdom and Japan and Newton Advanced Fellowship funding between the United Kingdom and China and Engineering and Physical Sciences Research Council UK for funding (Grant No. EP/W00562X/1). R.T. thanks the Indian Nanomission for a postdoctoral fellowship. A.M.S. thanks the SA-NRF and the URC/FRC of UJ for financial assistance.

[1] H. v. Löhneysen, A. Rosch, M. Vojta, and P. Wölfle, Fermi-liquid instabilities at magnetic quantum phase transitions, Rev. Mod. Phys. **79**, 1015 (2007).

[2] H. v. Löhneysen, C. Pfleiderer, T. Pietrus, O. Stockert, and B. Will, Pressure versus magnetic-field tuning of a magnetic quantum phase transition, Phys. Rev. B **63**, 134411 (2001).

[3] M. B. Maple, M. C. de Andrade, J. Herrmann, Y. Dalichaouch, D. A. Gajewski, C. L. Seaman, R. Chau, R. Movshovich, M. C. Aronson, and R. Osborn, Non Fermi liquid ground states in strongly correlated f-electron materials, J. Low Temp. Phys. **99**, 223 (1995).

[4] R. Tripathi, D. Das, C. Geibel, S. K. Dhar, and Z. Hossain, Non-Fermi-liquid behavior at the antiferromagnetic quantum critical point in the heavy-fermion system $Ce(Cu_{1-x}Co_x)_2Ge_2$, Phys. Rev. B **98**, 165136 (2018).

[5] N. D. Mathur, F. M. Grosche, S. R. Julian, I. R. Walker, D. M. Freye, R. K. W. Haselwimmer, and G. G. Lonzarich, Magnetically mediated superconductivity in heavy fermion compounds, Nature (London) **394**, 39 (1998).

[6] S. A. Grigera, R. S. Perry, A. J. Schofield, M. Chiao, S. R. Julian, G. G. Lonzarich, S. I. Ikeda, Y. Maeno, A. J. Millis, and A. P. Mackenzie, Magnetic field-tuned quantum criticality in the metallic ruthenate $Sr_3Ru_2O_7$, Science **294**, 329 (2001).

[7] G. R. Stewart, Non-Fermi-liquid behavior in d- and f-electron metals, Rev. Mod. Phys. **73**, 797 (2001).

[8] A. J. Schofield, Non-Fermi liquids, Contemp. Phys. **40**, 95 (1999).

[9] P. Gegenwart, Q. Si, and F. Steglich, Quantum criticality in heavy-fermion metals, Nat. Phys. **4**, 186 (2008).

[10] Q. Si and F. Steglich, Heavy fermions and quantum phase transitions, Science **329**, 1161 (2010).

[11] O. Stockert and F. Steglich, Unconventional quantum criticality in heavy-fermion compounds, Annu. Rev. Condens. Matter Phys. **2**, 79 (2011).

[12] A. Rosch, A. Schröder, O. Stockert, and H. v. Löhneysen, Mechanism for the non-Fermi-liquid behavior in $CeCu_{6-x}Au_x$, Phys. Rev. Lett. **79**, 159 (1997).

[13] O. O. Bernal, D. E. MacLaughlin, H. G. Lukefahr, and B. Andraka, Copper NMR and thermodynamics of $UCu_{5-x}Pd_x$: Evidence for kondo disorder, Phys. Rev. Lett. **75**, 2023 (1995).

[14] E. Miranda, V. Dobrosavljevic, and G. Kotliar, Kondo disorder: a possible route towards non-Fermi-liquid behaviour, J. Phys.: Condens. Matter **8**, 9871 (1996).

[15] A. H. Castro Neto, G. Castilla, and B. A. Jones, Non-Fermi liquid behavior and griffiths phase in f-electron compounds, Phys. Rev. Lett. **81**, 3531 (1998).

[16] A. H. Castro Neto and B. A. Jones, Non-Fermi-liquid behavior in U and Ce alloys: Criticality, disorder, dissipation, and Griffiths-McCoy singularities, Phys. Rev. B **62**, 14975 (2000).

[17] M. C. de Andrade, R. Chau, R. P. Dickey, N. R. Dilley, E. J. Freeman, D. A. Gajewski, M. B. Maple, R. Movshovich, A. H. Castro Neto, G. Castilla, and B. A. Jones, Evidence for a common physical description of non-Fermi-liquid behavior in chemically substituted f-electron systems, Phys. Rev. Lett. **81**, 5620 (1998).

[18] Y. Tabata, T. Taniguchi, Y. Miyako, O. Tegus, A. A. Menovsky, and J. A. Mydosh, H/T scaling in disordered non-Fermi liquid materials $Ce(Ru_{1-x}Rh_x)_2Si_2$ for $x = 0.5$ and 0.6: Quantum Griffiths nature, Phys. Rev. B **70**, 144415 (2004).

[19] B.-L. Young, D. E. MacLaughlin, M. S. Rose, K. Ishida, O. O. Bernal, H. G. Lukefahr, K. Heuser, G. R. Stewart, N. P. Butch, P.-C. Ho, and M. B. Maple, Disorder effects near a magnetic instability in $CePtSi_{1-x}Ge_x$ ($x = 0, 0.1$), Phys. Rev. B **70**, 024401 (2004).

[20] S. Raymond and D. Jaccard, Electronic properties of $CePd_2Si_2$ under pressure, Phys. Rev. B **61**, 8679 (2000).

[21] P. Gegenwart, F. Kromer, M. Lang, G. Sparn, C. Geibel, and F. Steglich, Non-Fermi-liquid effects at ambient pressure in a stoichiometric heavy-fermion compound with very low disorder: $CeNi_2Ge_2$, Phys. Rev. Lett. **82**, 1293 (1999).

[22] V. K. Anand, D. T. Adroja, A. D. Hillier, K. Shigetoh, T. Takabatake, J.-G. Park, K. A. McEwen, J. H. Pixley, and Q. Si, Zero-field ambient-pressure quantum criticality in the stoichiometric non-Fermi liquid system CeRhBi, J. Phys. Soc. Jpn. **87**, 064708 (2018).

[23] A. P. Ramirez, P. Chandra, P. Coleman, Z. Fisk, J. L. Smith, and H. R. Ott, Nonlinear susceptibility: A direct test of the quadrupolar kondo effect in UBe_{13}, Phys. Rev. Lett. **73**, 3018 (1994).

[24] Y. Matsumoto, S. Nakatsuji, K. Kuga, Y. Karaki, N. Horie, Y. Shimura, T. Sakakibara, A. H. Nevidomskyy, and P. Coleman, Quantum criticality without tuning in the mixed valence compound β-$YbAlB_4$, Science **331**, 316 (2011).

[25] A. J. Millis, Effect of a nonzero temperature on quantum critical points in itinerant fermion systems, Phys. Rev. B **48**, 7183 (1993).

[26] S. Nesterenko, V. Avzuragova, A. Tursina, and A. Strydom, New ternary aluminides $ReRh_4Al_{15}$ (Re = La, Ce, Pr, Sm, Gd), J. Alloys Compd. **792**, 1061 (2019).

[27] G. M. Sheldrick, Crystal structure refinement with *SHELXL*, Acta Cryst. C **71**, 3 (2015).

[28] L. M. Gelat and E. Parthe, Structure tidy – A computer program to standardize crystal structure data, J. Appl. Cryst. **20**, 139 (1987).

[29] O. Arnold, J. C. Bilheux, J. M. Borreguero, A. Buts, S. I. Campbell, L. Chapon, M. Doucet, N. Draper, R. Ferraz Leal, M. A. Gigg, V. E. Lynch, A. Markvardsen, D. J. Mikkelson, R. L. Mikkelson, R. Miller, K. Palmen, P. Parker, G. Passos, T. G. Perring, P. F. Peterson, S. Ren, M. A. Reuter, A. T. Savici, J. W. Taylor, R. J. Taylor, R. Tolchenov, W. Zhou, and J. Zikovsky, Mantid-data analysis and visualization package for neutron scattering and μSR experiments, Nucl. Instrum. Methods Phys. Res. Sect. A **764**, 156 (2014).

[30] F. Pratt, WIMDA: A muon data analysis program for the Windows PC, Physica B: Condens. Matter **289–290**, 710 (2000).

[31] R. I. Bewley, T. Guidi, and S. M. Bennington, Merlin: A high count rate chopper spectrometer at isis, Not. Neutroni Luce Sincrotrone **14**, 22 (2009).

[32] T. Sasakawa, K. Shigetoh, D. Hirata, K. Umeo, and T. Takabatake, Non-Fermi-liquid behavior in CeRhBi and valence-fluctuating behavior in CeIrSb, Physica B: Condens. Matter **359–361**, 111 (2005).

[33] A. Bhattacharyya, D. T. Adroja, J. S. Lord, L. Wang, Y. Shi, K. Panda, H. Luo, and A. M. Strydom, Quantum fluctuations in the quasi-one-dimensional non-Fermi liquid system $CeCo_2Ga_8$ investigated using μSR, Phys. Rev. B **101**, 214437 (2020).

[34] B. Andraka and A. M. Tsvelik, Observation of non-Fermi-liquid behavior in $U_{0.2}Y_{0.8}Pd_3$, Phys. Rev. Lett. **67**, 2886 (1991).

[35] A. M. Tsvelik and M. Reizer, Phenomenological theory of non-Fermi-liquid heavy-fermion alloys, Phys. Rev. B **48**, 9887 (1993).

[36] B. Andraka, Anomalous specific heat of $Ce_{1-x}Th_xRhSb$ alloys, Phys. Rev. B **49**, 348 (1994).

[37] A. D. Hillier, D. T. Adroja, S. R. Giblin, W. Kockelmann, B. D. Rainford, and S. K. Malik, Understanding the heavy fermion behavior in $CeInPt_4$, Phys. Rev. B **76**, 174439 (2007).

[38] H. v. Löhneysen, T. Pietrus, G. Portisch, H. G. Schlager, A. Schröder, M. Sieck, and T. Trappmann, Non-Fermi-liquid behavior in a heavy-fermion alloy at a magnetic instability, Phys. Rev. Lett. **72**, 3262 (1994).

[39] M. A. López de la Torre, J. A. González, A. Izquierdo, S. Vieira, M. Ellerby, and K. A. McEwen, On the relevance of Kondo disorder in the non-Fermi-liquid behavior of UCu_4Ni, J. Appl. Phys. **87**, 5126 (2000).

[40] M. Sasaki, A. Ohnishi, T. Kikuchi, M. Kitaura, K.-S. Kim, and H.-J. Kim, Interplay between the Kondo effect and randomness: Griffiths phase in M_xTiSe_2 (M = Co, Ni, and Fe) single crystals, Phys. Rev. B **82**, 224416 (2010).

[41] D. Nozadze and T. Vojta, Transport properties in antiferromagnetic quantum Griffiths phases, Europhys. Lett. **95**, 57010 (2011).

[42] P. Gegenwart, C. Langhammer, C. Geibel, R. Helfrich, M. Lang, G. Sparn, F. Steglich, R. Horn, L. Donnevert, A. Link, and W. Assmus, Breakup of heavy fermions on the brink of "phase A" in $CeCu_2Si_2$, Phys. Rev. Lett. **81**, 1501 (1998).

[43] O. Trovarelli, C. Geibel, S. Mederle, C. Langhammer, F. M. Grosche, P. Gegenwart, M. Lang, G. Sparn, and F. Steglich, $YbRh_2Si_2$: Pronounced non-Fermi-liquid effects above a low-lying magnetic phase transition, Phys. Rev. Lett. **85**, 626 (2000).

[44] S. R. Julian, C. Pfleiderer, F. M. Grosche, N. D. Mathur, G. J. McMullan, A. J. Diver, I. R. Walker, and G. G. Lonzarich, The normal states of magnetic d and f transition metals, J. Phys.: Condens. Matter **8**, 9675 (1996).

[45] P. Coleman, C. Pépin, Q. Si, and R. Ramazashvili, How do fermi liquids get heavy and die?, J. Phys.: Condens. Matter **13**, R723 (2001).

[46] P. Schlottmann, Bethe-ansatz solution of the ground-state of the SU(2j + 1) Kondo (coqblin-schrieffer) model: Magnetization, magnetoresistance and universality, Z. Phys. B **51**, 223 (1983).

[47] B. Zeng, Q. R. Zhang, D. Rhodes, Y. Shimura, D. Watanabe, R. E. Baumbach, P. Schlottmann, T. Ebihara, and L. Balicas, $CeCu_2Ge_2$: Challenging our understanding of quantum criticality, Phys. Rev. B **90**, 155101 (2014).

[48] Z. Hossain, S. Hamashima, K. Umeo, T. Takabatake, C. Geibel, and F. Steglich, Antiferromagnetic transitions in the Kondo lattice system $Ce_2Ni_3Ge_5$, Phys. Rev. B **62**, 8950 (2000).

[49] S. L. Lee, S. H. Kilcoyne, and R. Cywinski, Muon science: Muons in physics, chemistry and materials, in *Proceedings of the Fifty-First Scottish Universities Summer School in Physics*, NATO Advanced Study Institute (SUSSP, Edinburgh, UK, 1999).

[50] R. S. Hayano, Y. J. Uemura, J. Imazato, N. Nishida, T. Yamazaki, and R. Kubo, Zero-and low-field spin relaxation studied by positive muons, Phys. Rev. B **20**, 850 (1979).

[51] D. E. MacLaughlin, O. O. Bernal, R. H. Heffner, G. J. Nieuwenhuys, M. S. Rose, J. E. Sonier, B. Andraka, R. Chau, and M. B. Maple, Glassy spin dynamics in non-Fermi-liquid $UCu_{5-x}Pd_x$, $x = 1.0$ and 1.5, Phys. Rev. Lett. **87**, 066402 (2001).

[52] D. E. MacLaughlin, R. H. Heffner, O. O. Bernal, K. Ishida, J. E. Sonier, G. J. Nieuwenhuys, M. B. Maple, and G. R. Stewart, Disorder, inhomogeneity and spin dynamics in f-electron non-Fermi liquid systems, J. Phys.: Condens. Matter **16**, S4479 (2004).

[53] A. Keren, P. Mendels, I. A. Campbell, and J. Lord, Probing the spin-spin dynamical autocorrelation function in a spin glass above T_g via muon spin relaxation, Phys. Rev. Lett. **77**, 1386 (1996).

[54] D. R. Grempel and M. J. Rozenberg, On-Fermi-liquid behavior in a disordered Kondo-Alloy model, Phys. Rev. B **60**, 4702 (1999).

[55] R. Tripathi, D. Das, P. K. Biswas, D. T. Adroja, A. D. Hillier, and Z. Hossain, Quantum Griffiths phase near an antiferromagnetic quantum critical point: Muon spin relaxation study of $Ce(Cu_{1-x}Co_x)_2Ge_2$, Phys. Rev. B **99**, 224424 (2019).

[56] D. T. Adroja, A. D. Hillier, J.-G. Park, W. Kockelmann, K. A. McEwen, B. D. Rainford, K.-H. Jang, C. Geibel, and T. Takabatake, Muon spin relaxation study of non-Fermi-liquid behavior near the ferromagnetic quantum critical point in $CePd_{0.15}Rh_{0.85}$, Phys. Rev. B **78**, 014412 (2008).

[57] A. Keren, G. Bazalitsky, I. Campbell, and J. S. Lord, Probing exotic spin correlations by muon spin depolarization measurements with applications to spin glass dynamics, Phys. Rev. B **64**, 054403 (2001).

[58] A. P. Murani, Paramagnetic scattering from the valence-fluctuation compound $YbAl_3$, Phys. Rev. B **50**, 9882 (1994).

[59] K. W. H. Stevens, Matrix elements and operator equivalents connected with the magnetic properties of rare earth ions, Proc. Phys. Soc. A **65**, 209 (1952).

[60] S. Koerner, E.-W. Scheidt, T. Schreiner, K. Heuser, and G. R. Stewart, Crossover to Fermi-liquid behavior at lowest temperatures in pure $CeNi_2Ge_2$, J. Low Temp. Phys. **119**, 147 (2000).

[61] D. Adroja, S. Sharma, Y. Muro, A. Sundaresan, T. Takabatake, S. Langridge, and A. Strydom, Crystal field excitations to understand anisotropy behavior in new Ce based heavy fermions CeT_4Al_{15} (T=Rh and Ir) (2019), doi: 10.5286/ISIS.E.RB1920702.

[62] S. Sharma, D. Adroja, and P. Biswas, Investigating the quantum critical behavior of heavy fermion $CeRh_4Al_{15}$ (2020), doi: 10.5286/ISIS.E.RB2010778.